J. Phys. Chem. Solids, 1971, Vol. 32, pp. 2311–2330. Pergamon Press. Printed in Great Britain.

SHOCK-WAVE COMPRESSION OF SAPPHIRE FROM 15 TO 420 KBAR. THE EFFECTS OF LARGE ANISOTROPIC COMPRESSIONS*

R. A. GRAHAM and W. P. BROOKS
Sandia Laboratories, Albuquerque, New Mexico

(*Received* 14 *January* 1971)

Abstract—Under shock compression, sapphire (crystalline Al_2O_3) exhibits Hugoniot elastic limit, HEL, values of from 120–210 kbar; the largest values observed for any solid. Because of the large HEL, the stress configuration of the shock-loaded sample is highly anisotropic. A critical examination of the effects of large anisotropic stresses on the compression of solids is accomplished with shock experiments on sapphire in three crystallographic directions at stress values within the elastic range to stress values up to twice the HEL. The maximum shear strengths observed range from 4·9 to 5·6 per cent of the shear modulus. When stresses in excess of the HEL are achieved, sapphire is observed to undergo a catastropic loss of shear strength; in contrast to the yield behavior observed for metals. The results are compared to observations on high density polycrystalline Al_2O_3 and other solids with large HEL values. The behavior of sapphire is found to be analogous to that previously observed for crystalline SiO_2. Data in the elastic range show a third order elastic constant $C_{111} \approx C_{333} = -(3{\cdot}6 \pm 0{\cdot}4) \times 10^{13}$ dyne/cm^2. Analytical methods are developed to determine the shear stress offset independent of the hydrostatic data.

1. INTRODUCTION

COMPRESSION measurements for hydrostatic pressures greater than a few tens of kbars are difficult to accomplish and limited in accuracy [1]. Ultrasonic measurements of compressibility and its pressure derivative can be precisely determined but are limited to modest pressures [2]. Consequently, shock-wave compression measurements, which may be accomplished at very high pressures, are frequently employed to provide data which may be used to calculate high pressure isothermal compression curves [3] or to test extrapolation of ultrasonic data to very high pressure [2]. Unfortunately, data from shock compression experiments are not directly comparable to either ultrasonic data or static high pressure isothermal data. The experimental conditions of the shock experiment not only include heating due to the rapid compression but also include a potentially large shear stress component which is an inherent property depending upon the shear strength of the solid. Early shock compression workers usually assumed that the shear strength of solids was negligible so that the shock compression was isotropic and the calculation of an isothermal compression curve from the shock data was concerned only with thermodynamics of the shock heating and the equation-of-state of the solid [4]. It is now widely recognized that the effect of shear strength of the solid must be evaluated before hydrostatic and shock compression data can be directly compared. Unfortunately, the shear strengths of solids under shock-wave compression have not received as much study as thermodynamic effects and are not well enough understood to evaluate their effects unequivocally.

The object of the present paper is to evaluate shear strength effects in solids which exhibit unusually large shear strengths with correspondingly large anisotropic compressions. After introducing basic concepts of the stress configurations imposed by shock-loading and

*Work supported by the U.S. Atomic Energy Commission.

JAN 10 1972

the shear strength, the existing models for the effects of shear strength of solids on the compressions experienced in a shock compression experiment will be reviewed. Following this, an experimental study of the shock compression of sapphire (single crystal Al_2O_3) will be described and the results will be presented and examined for shear strength effects. A determination of several higher-order elastic constants will also be presented. The results of the present investigation will then be used along with the other data in the literature to assess the present understanding of shear strength effects in solids under shock compression.

2. BACKGROUND

(a) *Shear strength of solids*

Shock loading a sample with the detonation of a high explosive[5], the impact of a projectile[6, 7], or the rapid deposition of radiant energy[8] produces an inertial response with pressures and pressure-time histories which depend upon the compressional properties of the sample. When the sample is loaded over a large planar area the compression is uniaxial, i.e., a state of uniaxial strain is achieved for times less than that required for unloading pulses to arrive in the test area. If the sample has a finite, i.e., non-zero, shear strength, the stress configuration is not isotropic since the resulting inertial stress components normal to the shock compression direction are less than the stress component in the shock propagation, or axial, direction. The shock experiment measures only the stress component in the axial direction while the lateral stress components can only be inferred by indirect means. Moreover, the axial component of stress will be larger than the isotropic pressure at the same compression to an extent depending upon the magnitude of the shear component of stress. The relation between the isotropic and anisotropic compressions must be known before the shock data can be converted to equivalent isotropic compression conditions.

The magnitude of the shear may be expressed in terms of the stress component, σ_x, measured in the shock experiment and a mean pressure value by considering an anisotropic stress configuration and defining a mean pressure, $\bar{P}$, as

$$\bar{P} \equiv \tfrac{1}{3}(\sigma_x+\sigma_y+\sigma_z). \tag{1}$$

If a solid is laterally isotropic the lateral stress components are equal, i.e., $\sigma_y = \sigma_z$. Equation (1) may then be rearranged such that

$$\bar{P} = \sigma_x - \tfrac{2}{3}(\sigma_x-\sigma_z). \tag{2}$$

The maximum value of the shear stress, τ_{max}, is

$$\tau_{max} = \tfrac{1}{2}(\sigma_x-\sigma_z), \tag{3}$$

thus,

$$\bar{P} = \sigma_x - \tfrac{4}{3}\tau_{max}. \tag{4}$$

It will be convenient in what follows to refer to the difference between σ_x and $\bar{P}$ as the *shear stress offset* defined as

$$\sigma_\tau \equiv \sigma_x - \bar{P}. \tag{5}$$

The determination of differences between longitudinal shock compression stresses, σ_x, and hydrostatic pressures, P, at the same volume could provide an experimental measure of the shear stress offset. However, as previously indicated, measurements of both σ_x and P are normally not available in the same high pressure range and it is desirable to evaluate σ_τ independently so that measurements of σ_x may be used to compute $\bar{P}$.

Since the strain configuration is known to be uniaxial and since solids are frequently observed to behave elastically up to a yield stress value in shock compression called the Hugoniot elastic limit, HEL, the shear stress value at the HEL can be computed assuming that Hooke's law is valid. In this case

$$\tau^* = \tfrac{1}{2}[(1-2\nu)/(1-\nu)]\sigma_H \tag{6}$$

where τ^* is the limiting shear imposed by the shear strength of the solid as computed from the measured HEL, σ_H, and ν is Poisson's ratio for the solid. It is convenient to define a *shear strength offset*

$$\sigma^* \equiv \tfrac{4}{3}\tau^* \tag{7}$$

in a like manner to the shear stress offset σ_τ.

In this paper the high pressure region above the HEL will be examined to determine the magnitude of the *shear stress offset*, σ_τ, and its relation to the *shear strength offset*, σ^*. Previous theoretical and experimental studies have indicated the basis for two radically different relations between σ_τ and σ^*. These relations are developed for *elastic-plastic solids* and what will be called *elastic-isotropic solids*.

(b) *The elastic–plastic solid*

The theory of plasticity has been adapted to the uniaxial strain configuration in studies by Wood[9] and Fowles[10]. One result which may be extracted from this work is that under ideally plastic deformation

$$\sigma_\tau = \sigma^*, \qquad \sigma_\tau > \sigma_H; \tag{8}$$

that is, the shear stress offset is independent of pressure and equals the shear strength offset which is a fixed property of the solid. For the elastic–plastic solid the magnitude of the shear stress has no inherent effect on the properties of the solid and the solid can be characterized as having a constant shear strength.

The elastic–plastic solid has very attractive features since it is particularly simple in concept both theoretically and phenomenologically and the numerous static studies of plastic flow and deformation can be used as a guide for the shock deformation. Furthermore, the microscopic theories of dislocation motion in solids have been successful in explaining many aspects of plastic flow under static conditions and similar dislocation theories have been successfully pursued under shock loading. This provides a fundamental basis for understanding the response of solids to large anisotropic compressions and second-order effects involving small changes in σ_τ. In addition, rate effects observed in shock experiments may be described in terms of the dislocation theory.

Since the initial experimental confirmation of elastic-plastic response of aluminum by Fowles[10] in 1961, several experimental investigations have demonstrated that a number of metals respond to shock loading as elastic–plastic solids[11–18]. In addition a recent examination of the fixed point phase transition pressures measured under hydrostatic and shock conditions indicated that the elastic–plastic model correctly correlated the shock and static results for a number of metals [19]. Although numerous deviations to the elastic–plastic response of metals have been noted, such as different HEL values than predicted from static measurements[20, 21] and unloading paths[22] not predicted by elastic plastic response, it appears likely that they can be explained in terms of modifications to the basic theory.

Confirmation of the elastic plastic model is particularly gratifying since HEL values can be routinely measured experimentally and the HEL value can be used to calculate σ_τ if elastic–plastic response correctly describes the solid. Furthermore a recent survey of HEL values[20] indicates that shear strength effects are not negligible in many instances.

Unaware of the simplicity of the elastic–plastic response, crystalline quartz chooses to respond to anisotropic compressions in a radically different fashion, thereby raising questions as to the generality of the elastic–plastic response, and the calculation of σ_τ from the measured HEL values.

(c) *The elastic–isotropic solid*

Shock experiments on single crystal quartz revealed an unexpected and dramatically different response than that observed for

metals. Neilson and Benedick[23] conducted experiments in which X-cut quartz was shock-loaded at high pressures and the resulting piezoelectric outputs were measured. Interpretation of these piezoelectric outputs required that quartz exhibit an unusually large HEL and a state of zero piezoelectric polarization in the high pressure region above the HEL. The piezoelectric response of quartz to isotropic compression is zero; hence, zero polarization requires $\sigma_\tau = 0$. This observation led Wackerle[24] and Fowles[25] to perform shock compression measurements on crystalline quartz which, when compared with Bridgman's hydrostatic data, showed that even though σ^* was unusually large, that $\sigma_\tau = 0$ for stresses greater than the HEL. The manner in which quartz suffers this loss of shear strength seems inexplicable within the theory of plasticity and classical dislocation mechanics. Unlike the elastic–plastic solid which has a fixed characteristic shear strength, the elastic–isotropic solid suffers a catastropic loss of shear strength when a critical shear stress is exceeded. The magnitude of the shear stress alters the shear properties of the solid.

The phenomenological difference between the elastic–plastic solid and the elastic–isotropic solid is demonstrated in Fig. 1. Unlike the elastic–plastic response which shows a constant offset from the isotropic compression curve above the HEL, the elastic–isotropic response shows no offset. If the process by which the loss of shear strength occurs does not alter properties of the solid, the hydrostatic compression curve and shock compression curve will be the same in regions where the shock heating is negligible.

In contrast to the situation for metals, the generality of the loss of shear strength has not been systematically explored. It has been suggested[26, 27] that the elastic–isotropic response may be typical of 'brittle' solids but little systematic attempt has been made to verify this characterization.

Recently, Ahrens *et al.*[28], reported

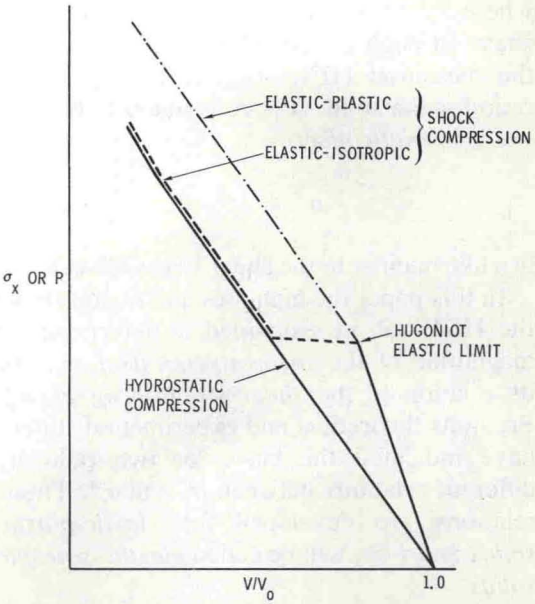

Fig. 1. Principal features of the two simplest models for the compressional behavior of solids under shock compression. The elastic–plastic solid exhibits a constant shear stress offset from the hydrostatic curve for stresses greater than the HEL. On the other hand, the elastic–isotropic solid exhibits no shear stress offset. Unlike the elastic–plastic solid, the shear strength of the elastic–isotropic solid is irreversibly reduced by the shear stress accompanying uniaxial strain.

shock-compression measurements on a high-density polycrystalline Al_2O_3 and concluded that Al_2O_3 responded as an elastic–plastic solid. This was subsequently confirmed by Munson[29]. Since polycrystalline Al_2O_3 is a brittle solid this observation is not consistent with the early predictions of the response of brittle solids. Further complicating the question, McWhan[30] reported static compression measurements on quartz with X-ray techniques and found that the shock data and the high pressure static data showed a small, 1 per cent offset in volume. Thus, at the present time we have no consistent basis for predicting the shear stress offsets of solids other than metals and are faced with a fundamental unknown in the mechanical response of solids to large anisotropic compressions.

The present study of the shock compression of single crystal Al_2O_3, sapphire, was under-

taken to examine further the effects of large anisotropic compressions resulting from large values of the HEL[31]. Analytical methods developed in the discussion section give an explicit basis for identification of the loss of shear strength under shock loading. Sapphire is an excellent material for further study because it has similar characteristics to quartz. Both crystals are oxides, both crystals are trigonal; however, sapphire has much larger values for elastic constants. Furthermore, the shear strength effects for sapphire are larger than thermal effects thus affording an uncoupling between mechanical and thermal effects.

Even though the principal interest of this investigation is in the high pressure region above the HEL, measurements were accomplished both below and above the HEL. The measurements below the HEL permit an examination of several elastic constants at compressions an order of magnitude larger than those previously employed and help to guide the extrapolation of the ultrasonic data to the high pressure region.

3. EXPERIMENTAL ARRANGEMENTS

The experiments were of two basic types; those which determined the high pressure response above the Hugoniot elastic limit, HEL, and those which determined the elastic response below the HEL. The high pressure experiments utilized shock-loading with plane wave high explosive techniques, while the elastic response was determined in experiments which utilized projectile impact loading techniques.

The high pressure experiments were accomplished by generating explosively driven plane shock-waves into the samples and monitoring their response with an optical technique similar to that employed by Wackerle[24]. A schematic of this experimental arrangement is shown in Fig. 2. The high explosive plane-wave generators and explosive pads send a shock wave from the detonation through an intermediate driver plate of 2024 aluminum and into the disk-shaped sample. Various pressures are then achieved by the choice of different high explosive materials. The various explosive and impact configurations are described in Table 1.

During the experiment the position of the wire and its image are viewed through appropriate lenses through a 0·1 mm observation slit in the camera and recorded on film as a function of time as the shock wave enters the sample and reflects from the free surface. As the shock enters the sample, the reflectivity of the input surface plating is destroyed and the background light intensity is abruptly changed. An alternate transit time measurement with quartz pins was necessary because of the unreliable nature of the change in reflectivity as the shock entered the sample. The sharp extinction in background light was not always achieved.

After arrival of the second wave the image was sometimes optically distorted as shown in Fig. 2 by the opening of minute scratches on the polished surface. In these cases, however, the scratches themselves or the edge of reflecting surface follow the surface motion directly and their motion was used to obtain second-wave free-surface velocity measurements.

The calibrations of displacement and time are particularly simplified in this technique. The position of the wire above the free surface is measured before shot time to one part in 10^4. The displacement magnitude is then indicated directly on the film by the distance between the wire and its image before shock arrival at the free surface. The rotation speed of the rotating mirror in the camera was measured at shot-time with a resulting sweep rate accurate to $\pm\frac{1}{2}$ per cent. Consideration of all the possible experimental errors in measurements and data reduction gives estimated errors of ± 1 to 2 per cent in shock velocity and ± 3 per cent in free-surface velocity.

The samples used in the high pressure experiments were cut from single crystal boules of sapphire grown by the Verneuil technique

Table 1. *Shock loading configurations*

Designation	Configuration	Measurements
H	Gun-symmetric impact	impact velocity electrical response
HQ	Gun-quartz gauge	impact velocity quartz gauge signals
B	*P*-40[a] + 25 mm Baratol[b] plus 12 mm 2024 aluminum alloy	free surface velocity (optical) shock velocity (optical/and/or quartz pins)
T	*P*-40[a] + 25 mm TNT plus 12 mm 2024 aluminum alloy	"
C	*P*-40[a] + 25 mm Composition B plus 12 mm 2024 aluminum alloy	"
H	*P*-40[a] + 25 mm PBX 9404 plus 12 mm 2024 aluminum alloy	"

[a]Designation for 10 cm dia. plane wave explosive lens as described in Ref. [5].
[b]Explosive compositions are further described in Ref. [5].

by the Linde Co. The samples were cut, crystallographically oriented, and polished by the Valpey Corporation. The disks were nominally 31 mm in diameter and 6, 10 or 13 mm in thickness. The material was clean and free of defects to the unaided eye. Crystallographic orientations investigated were the natural growth direction of 60°, the optical orientation 0° as well as the 90° orientation.*

Experiments below the HEL were accomplished utilizing the symmetrical projectile impact and electrical response technique previously discussed in some detail[32]. The sample disk is mounted on the impact face of a high velocity compressed gas gun and impacted with a projectile faced with another sample disk. Because of the symmetry of the impacting samples, the particle velocity imparted to the sample is precisely one-half the measured impact velocity. The shock-wave velocity at various particle velocities is measured by observing the electrical response of the sample which is initially charged to a high voltage. The transit time of the shock is clearly indicated on the electrical response records. This experiment is especially useful for determining the shock compression in the elastic range. Experiments beginning at low stress levels and increasing in stress amplitude help to insure the proper identification of the elastic-wave in the high pressure experiments.

One critical projectile impact experiment was performed with Sandia quartz shock-wave stress gauges[33] in which both the impact surface response and back surface response is precisely monitored in time. This type of experiment which has been previously described[34] provides superior time-resolution of the stress profiles in the sample.

4. RESULTS

Measurements and data analysis for shock compression experiments are concerned with the description of the stress vs. time or stress vs. position profiles which result when one surface of a plane sample is subjected to various transient high pressure loadings. The characteristics of these profiles can be shown to be directly related to the stress vs. com-

*The crystallographic orientation of the 0° axis is [0001], for the 90° axis is $[\bar{1}2\bar{1}0]$ and for the 60° axis is $[11\bar{2}3]$.

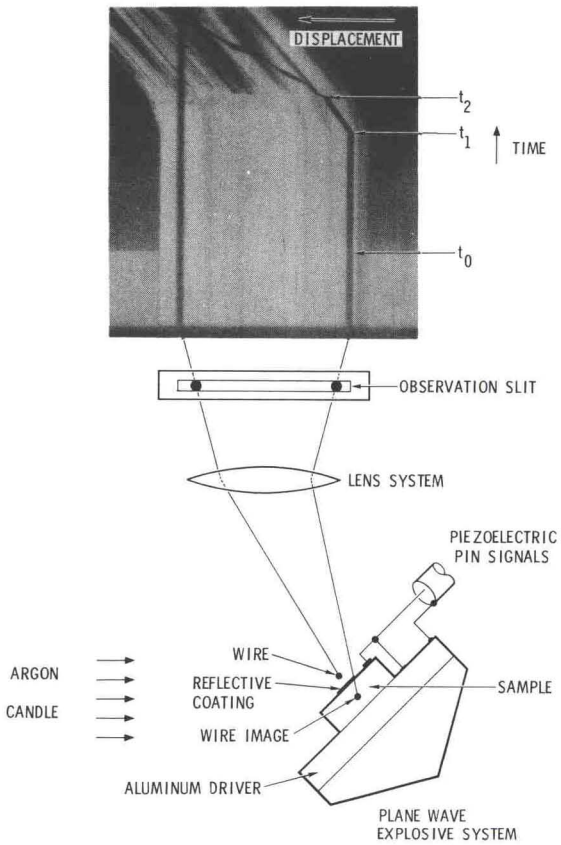

Fig. 2. Experimental technique used in the high pressure experiments. The displacement vs. time response of the free surface of the sample to high explosive loading is monitored with a high speed streak camera which follows the motion of a 0·1 mm dia. wire and its image as reflected from the surface of the sample. The high speed camera was a Beckman and Whitley Model 770 with a maximum writing speed of 16·7 mm/μsec. Shock arrival times of the first waves are also monitored with piezoelectric pins. The typical record shows the extinction of background light when the shock enters the sample at time t_0. The arrival time of the first wave at the free surface is t_1 and the arrival time of the second wave is at t_2. For the experimental record shown, the time difference $t_1 - t_0$ is 1·077 μsec and the height of the wire above the sample is 1·610 mm.

[*Facing page* 2316]

pression curve for the sample material. In the present paper two characteristically different wave profiles are observed in the various stress ranges. These are (1) a single elastic compressive wave of stress less than the HEL and (2) a two-shock front profile consisting of an elastic wave, whose amplitude is the HEL, and a slower moving higher pressure wave. Since different assumptions are employed in the data reduction in each of the two cases the method of data reduction for each experiment will be described.

The stress vs. compression states for each experiment are calculated assuming steady wave conditions and applying the conservation of mass and momentum conditions across each shock front. Thus, from the conservation of mass

$$\frac{\Delta V}{V_0} \equiv \eta = \frac{\Delta u}{U - u_i}, \tag{9}$$

and from the conservation of momentum

$$\Delta\sigma = \rho_0 (U - u_i)\Delta u, \tag{10}$$

where V_0 is the specific volume ahead of a shock front, ΔV is the magnitude of the change in specific volume imparted by the shock front, η is the strain or compression, Δu is the change in particle velocity, u_i is the particle velocity ahead of the shock front, $\Delta\sigma$ is the change in stress imparted by the shock front in a direction normal to the shock front. All velocities are in laboratory coordinates.

(a) *Elastic range experiments*

Experiments conducted within the elastic range were accomplished with the symmetrical impact configuration. Under these conditions a single shock front propagates with amplitude equal to the input particle velocity and travels with a fixed shock propagation velocity. In the experiment the particle velocity is measured with an accuracy of $\pm 0{\cdot}3$ per cent while the shock velocity is measured with an accuracy of ± 1 to $1-\frac{1}{2}$ per cent. These values should be contrasted to the explosively driven experiments which produce multiple shock fronts whose free-surface velocities are measured with an accuracy of ± 3 per cent while the shock propagation velocities are measured with an accuracy of 1 to 2 per cent.

The shock velocity and particle velocity values observed are shown in Table 2 along with the computed stress and compression data. The experiments in the elastic range are conducted over a range of stress from 15 to 100 kbar with measurements in three crystallographic orientations. Typical records from which these data are obtained have been previously shown[32]. Increased shock velocity is observed with increasing particle velocity in all crystallographic orientations. This behavior will be compared to ultrasonic determinations of higher order elastic constants in the discussion section.

One special experiment was conducted on a 60° orientation sample. This crystallographic orientation is the natural growth direction of the artificially grown sapphire boules. For this reason, the availability, low cost and high quality of the material in the large diameters required for this work, make the 60° orientation more desirable than other orientations. On the other hand, this crystallographic orientation is apparently not a 'specific direction,' that is, a longitudinal motion applied along the disk axis may produce both a quasi-longitudinal and a quasi-shear wave[35]. However, even though sapphire has trigonal symmetry the elastic stiffnesses do not vary significantly with orientation. For example, the longitudinal wave speeds in the 0° and 90° orientations differ by only $\frac{1}{2}$ per cent. Hence, the nonsymmetric response would be expected to be small if not insignificant.

To determine the extent of the effect, a 60° orientation sample was impacted at 28 kbar with a quartz gauge which precisely measures the input stress to the sample. This same experiment also included a quartz gauge measurement of the resulting shock wave profile after propagation through a distance of

Table 2. Shock compression data for sapphire

$\rho_0 = 3{\cdot}986$ g cm^{-3}

Shot no.	Configuration	Sample thickness	First wave u_1	First wave U_1	First wave σ_1	First wave V_1/V_0	Second wave u_2	Second wave $\bar{U}_2$	Second wave U_2	Second wave σ_2	Second wave V_2/V_0
		mm	mm μsec^{-1}	^{mm} μsec^{-1}	kbar		mm μsec^{-1}	mm μsec^{-1}	mm μsec^{-1}	kbar	
				0° orientation							
H298	*H*	2·54	0·0333	11·29	15·2	0·9970					
H221	*H*	5·11	0·0401	11·2	17·9	0·9964					
H305	*H*	2·56	0·0463	11·1	21·3	0·9958					
H297	*H*	2·57	0·0810	11·25	36·7	0·9929					
H216	*H*	5·11	0·0943	11·2	42·1	0·9916					
H299	*H*	2·54	0·1122	11·3	50·4	0·9901					
132-65	*B*	10·89	0·38	11·65	175	0·9674	Second wave not observed				
134-66	*B*	10·90	0·34	(11·6)[a]	157	0·9707	Second wave not observed				
357-67	*B*	6·450	0·31	(11·5)[a]	142	0·9730	0·49	8·05	7·56	196	0·9488
331-65	*T*	12·70	0·30	11·55	138	0·9740	0·69	8·88	8·61	271	0·9283
379-67	*T*	6·400	0·32	11·6-11·4	148	0·9722	0·71	8·76	8·49	262	0·9258
330-65	*C*	10·86	0·33	11·55-11·6	150	0·9715	0·86	9·12	8·91	337	0·9114
663-66	*C*	6·401	0·37	11·5-11·4	170	0·9677	0·83	8·55	8·24	319	0·9111
160-65	*H*	12·68	0·41	11·77	195	0·9652	1·08	8·82	8·52	419	0·8855
380-67	*H*	6·400	0·46	11·64	210	0·9605	0·94	8·91	8·67	370	0·9029
				0° orientation							
H317	*H*	2·59	0·1213	11·2	52·6	0·9892					
H318	*H*	2·58	0·1477	11·2	64·1	0·9868					
178-66	*B*	10·86	0·342	11·39	155	0·9700	0·474	6·90	5·97	186	0·9472
546-65	*T*	10·89	0·291	11·57	134	0·9748	0·69	8·63	8·25	264	0·9259
545-65	*H*	10·80	0·381	11·76	179	0·9676	0·98	8·72	8·44	378	0·8957
				60° orientation							
H245	*H*	3·21	0·0370	11·1	16·1	0·9967					
H267	*HQ*		0·0653		28·2	0·9943					
		12·67		11·16	28·5						
H248	*H*	3·21	0·0703	11·2	31·3	0·9937					
H246	*H*	3·19	0·0780	11·1	34·5	0·9930					
H250	*H*	3·20	0·1268	11·1	55·7	0·9886					
H211	*H*	3·15	0·225	11·2	102	0·9796					
192-64	*B*	12·832	0·267	11·23	120	0·9762	0·456	8·07	7·60	177	0·9510
257-64	*C*	12·750	0·374	11·38	170	0·9671	0·895	8·62	8·34	341	0·9034
219-66	*C*	12·800	0·35	11·43-11·40	160	0·9694	0·83	8·53	8·14	314	0·9097
188-64	*H*	12·817	0·282	11·54	130	0·9756	0·99	9·39	9·18	388	0·8980

[a]Not measured due to partial experimental failure.
Values shown are those assumed to calculate first wave parameters.

12 mm. The result is shown in Table 2 as shot No. H267. The input and output measurement agreed to within 1 per cent and the shock profile showed no dispersion in time. Thus, on the basis of this measurement the 60° orientation samples can be considered as exhibiting pure longitudinal wave propagation without detectable error in measurements or calculations.

(b) *High pressure experiments*

Analysis of the explosively-driven shock profile measurements requires a number of additional assumptions due to the reflection of the shocks from the free surface of the samples and the subsequent interaction of the reflected elastic wave with the slower moving high pressure wave. The arrival of the shock waves at the free-surface causes a complete reflection of the incident wave back into the bulk of the sample. If this reflection occurs symmetrically, the resulting free surface velocity is twice the incident particle velocity. This free-surface velocity assumption has been applied to compute the incident particle velocity from the measured free surface velocity. The interaction of this reflected elastic wave with the high pressure wave causes a detectable effect on the data analysis.

The high pressure wave is perturbed before it arrives at the measuring station; thus, the principal problem is to deduce the unperturbed second wave shock velocity from the measurements at the free surface. This interaction is a more important problem than that experienced in experiments on metals because of the possibility of the irreversible loss of shear strength at high pressures. A detailed and graphical description of the problem is given by Ahrens *et al.*[28] and is discussed for the similar situation in quartz by Wackerle [24] and Fowles [25].

Following Wackerle [24] the second wave propagation velocity, U_2, is calculated from the relation:

$$U_2 = \bar{U}_2\left[1-\frac{\Delta t}{t_1}\left\{\frac{(U_3-2u_1)(U_1-2u_1)t_2-U_1^2t_1}{U_1(U_3-2u_1)t_2+U_1^2t_1}\right\}\right] \tag{11}$$

where $\bar{U}_2$ is the nominal shock velocity taken as the original thickness, l, divided by the arrival time, t_2, of the second wave at the free surface, Δt is the difference in arrival times between the first and second waves, t_1 is the arrival time of the first wave, the u's are the particle velocities of the various waves as indicated by the subscripts, U_3 is the shock velocity of the reflected elastic wave after interaction with the second wave, and U_1 is the shock velocity of the first wave.

In the stress range just above the HEL the calculated value of U_2 is sensitive to the choice of a value for U_3 which is not measured in the experiment. However, even though U_2 cannot always be calculated unequivocally the uncertainty in U_3 is not sufficient to change any conclusions and only in the experiments 178-66, 357-67 and 192-64 does it affect the U_2 values significantly. In the data shown in Table 2 the value of U_3 is chosen to be U_1+2u_1, in accordance with the view that the material can be elastically reduced to zero stress and subsequently restressed to support the same HEL value. This assumption was found to lead to no inconsistencies among the data and among comparisons to other investigators data.

In order to examine the possibility of nonsteady material response accompanying the transition from elastic compression to inelastic compression, experiments were conducted at three sample thicknesses and for four different explosive driving pressures. Although no unequivocal evidence of stress relaxation was observed behind the elastic wave, the amplitude of the elastic wave, HEL, summarized in Table 3 shows both a thickness dependence and a driving pressure dependence which is characteristic of nonsteady behavior of the elastic wave. It is probable that small stress relaxation could occur and not be detected by the displacement-time measurements which are inherently

Table 3. Hugoniot elastic limits of sapphire

Driver	0° orientation	90° orientation	60° orientation
Sample thickness			
Baratol			
13 mm	—	—	120
11 mm	165*	155	—
6 mm	140	—	—
TNT			
13 mm	140	—	—
11 mm	—	135	—
6 mm	150	—	—
Comp B			
13 mm	—	—	—
11 mm	150	—	165*
6 mm	170	—	—
9404			
13 mm	195	—	130
11 mm	—	180	—
6 mm	210	—	—

*mean value of two experiments.

limited by poor resolution of rapid changes in velocity.

The values observed range from 120 to 210 kbar. Thus sapphire exhibits the largest HEL value ever observed for any material. There is considerable scatter in the HEL data. Examination of similar sapphire samples in polarized light indicated considerable internal strain in many samples and it appears that the scatter in HEL values results from the extent of the internal strain in the samples.

5. DISCUSSION

Because of the very large HEL values, the shock compression response for sapphire is well suited for use in studying the effects of large anisotropic compressions on solids. From the data in the elastic range, values for several third order elastic constants will be computed at substantially larger compressions than previously employed. From the data in the high pressure region above the HEL the shear stress configuration will be determined and conclusions drawn concerning the effect of shear on compressional behavior of solids. Finally, the HEL values themselves will be analyzed to provide a basis for predicting the conditions under which large values of HEL are observed. As indicated in the introduction the present understanding of these questions for solids other than the metals is inadequate even though these questions are important to our determinations of high pressure equations of state, physical property measurements under shock compressions, and a general theory of plasticity of solids.

This section will first compare the data in the elastic range to extrapolations of ultrasonic measurements of elastic constants. Following this, the high pressure data above the HEL will be examined for evidence of shear stress components and compared to the amplitudes of the HEL and to values for other solids.

(a) *Elastic range data*

The compressions achieved in the elastic range are an order of magnitude larger than those achieved in the recent ultrasonic measurements of Gieske and Barsch [36].

Unlike shock compression data at stresses greater than the HEL, uncertain effects of the stress configuration are minimal and interpretation of the data is more direct. Even though ultrasonic measurements are far more precise than shock compression techniques, the larger compressions of the shock experiment enhance higher order effects sufficiently to be observable.

Fowles[25] has recently demonstrated that Thurston's finite strain theory can be adapted so that shock compression data in the elastic range can be used along with ultrasonic data to determine higher order elastic constants. Fowles[25] developed an explicit stress vs. compression relation involving higher order elastic constants for large uniaxial elastic compression which we will use to interpret the shock compression data. In order to test the adequacy of the usual second order elastic constant description of sapphire at large compressions, the data of Gieske and Barsch are used to calculate the stress-volume relations from Fowles' finite strain development. The results of the calculations are shown in Fig. 3 along with the shock compression data. At the smaller compressions the different crystallographic orientations cannot be distinguished between at the scale of the figure and the differences at the largest compressions are less than the experimental error. Recent shock compression data of Barker *et al.*[37] on 0° sapphire are also included in the figure.

Examination of the extrapolated ultrasonic data in Fig. 3 shows a systematic deviation between the compression computed from second order constants and the observed shock compressions. The value of the third order elastic constant which gives the best fit to the shock data is obtained by determining the difference between the stress compression curve calculated from the second order constants and the observed shock compression data. Within the accuracy of the data, $C_{111} \approx C_{333} = -(3{\cdot}6 \pm 0{\cdot}4) \times 10^{13}$ dyne/cm^2.

Because third order elastic constants give sufficiently good description to the shock data, extrapolation of the ultrasonically measured bulk modulus and its pressure derivative should provide an accurate estimate of the isotropic compression curve for comparison with the shock compression data above the HEL.*

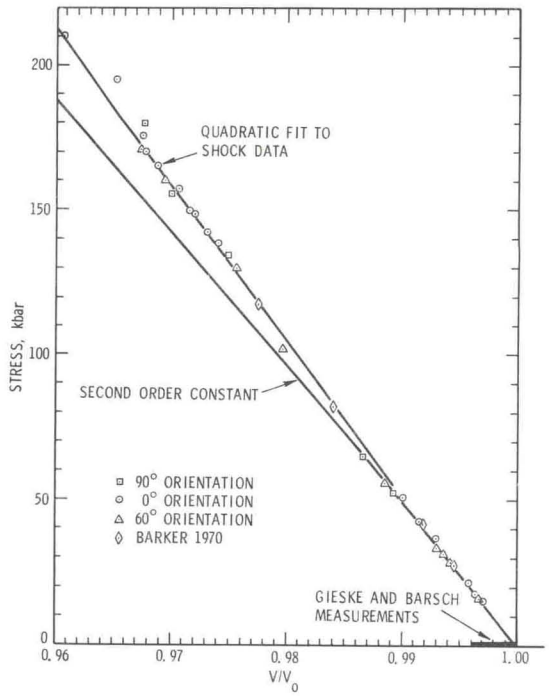

Fig. 3. Shock compression of sapphire in the elastic range. The second-order elastic constants of Gieske and Barsch are used in Fowles' finite strain equations to predict the large strain results in the 0° and 90° orientations indicated by the second order constant line. The slight negative curvature of the second order constant line is a result of finite strain theory. The difference between the shock results, as fit by a quadratic, and the finite strain values predicted from the usual second-order constant predictions allow third order elastic constants to be computed. Recent shock data of Barker are also included. To the scale used in the figure the compressions in the various crystallographic orientations cannot be distinguished between. The compression range of the hydrostatic pressure measurements of Gieske and Barsch are indicated along the abscissa.

(b) *High pressure response*

The unusually large HEL values observed for sapphire cause large deviations in stress-

*Note added in proof (See p. 2330).

volume relations from the isotropic compressions achieved in hydrostatic experiments. Furthermore the large shear stresses which are a consequence of the large HEL values cause concern that the shear itself may cause irreversible changes in the properties of the solid. Although it is possible to compare shock data directly with hydrostatic data as one method for determination of shear stress offset in the high pressure region, it is advantageous to develop techniques for determining shear strength from the shock data itself, independent of the hydrostatic data. Conclusions based on the study of the shock data alone impose no *a priori* assumptions concerning the equivalence of the shock and hydrostatic compressions and from a pragmatic point of view the conclusions are not susceptible to changes in the static data or uncertainties concerning the equation of state. Accordingly, we will delay comparing shock and static data until the shock data has been examined for evidence of shear stress offset.

(c) *Compression observations*

One of the most obvious and striking features of the data shown in Fig. 4 is that all the high pressure compression states fall on a common compression curve. The common compression curve is observed even though HEL values ranging from 120 to 210 kbar were observed for the different crystallographic orientations, sample thicknesses and driving pressures. According to the elastic–plastic model each high pressure experiment should exhibit a shear stress offset equal to the shear strength offset which is proportional to the HEL. Thus, different high pressure compression curves should be observed for different HEL values. The common compression curve indicates the constant shear strength model will not describe the response of sapphire. Although the value of the shear stress offset cannot be obtained from the observation of a common compression curve it is possible to conclude that sapphire experiences a substantial loss of shear strength and a collapse

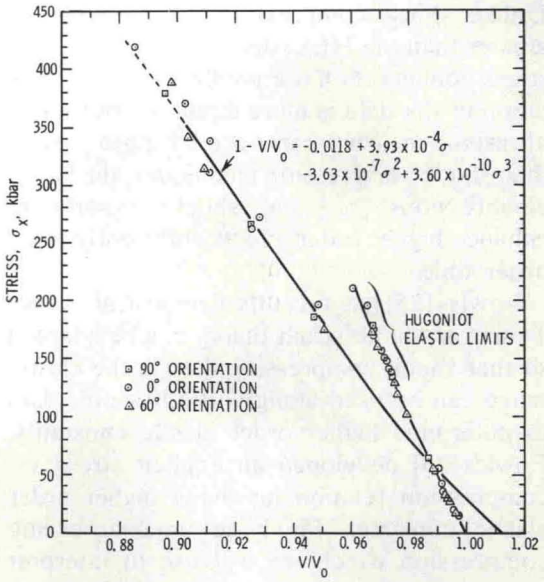

Fig. 4. Stress-volume relations for sapphire under shock-wave compression. The experimental points for the present investigation are fit with the cubic polynomial relation shown. All high pressure points show a common compression curve in spite of the fact that various Hugoniot elastic limits are observed depending upon the crystallographic orientation and driving pressure. For stresses above 350 kbar the data are not as accurately fit by the cubic polynomial.

toward the isotropic compression curve. The common compression curve, which is an explicit demonstration of a significant loss of shear strength, was also observed for shock-loaded crystalline quartz [24].

(d) *Shock velocity values*

The stress-volume conditions in the immediate vicinity of the HEL are a sensitive indication of changes in the shear strength in the high pressure region. This can be demonstrated by considering equation (5) which relates the longitudinal stress, σ_x, measured in the shock experiment to the mean pressure, $\bar{P}$, and the shear stress offset, σ_τ. The shock compressibility may be obtained from derivatives of equation (5) with volume such that

$$\frac{d\sigma_x}{dV} = \frac{d\bar{P}}{dV} + \frac{d\sigma_\tau}{dV}. \qquad (12)$$

A constant shear stress immediately above the HEL requires $d\sigma_\tau/dV = 0$. In this case the shock compressibility and isotropic compressibility are equal and a disturbance will travel with the bulk sound speed. On the other hand a significant change in σ_τ requires $d\sigma_\tau/dV \neq 0$ and a change in shock compressibility will result. If the shear strength is reduced the shock compressibility will be less than the isotropic compressibility and a disturbance will travel with a velocity less than bulk sound speed. In the absence of a phase transition this 'slow second-wave' is an explicit indication of large decreases in shear strength.

One of the experiments was conducted at a pressure just above the HEL. The second-wave shock velocity on experiment 178-66 is calculated to 6·0 mm/μsec compared to the bulk sound speed of 8·0 mm/μsec. Two other experiments (192-64 and 357-67) also showed shock velocities substantially less than bulk sound speed. The method of data reduction is admittedly subject to error because of the interaction of the first and second waves. However, the reduced data in experiment 178 cannot be changed sufficiently by various assumptions in the data analysis to obtain a shock velocity as large as the bulk sound speed. Thus, the slow second wave velocity data give a positive indication of the loss of shear strength for pressures just above the HEL.

Wackerle's shock compression study of crystalline quartz[24] also showed one experiment in which the shock velocity was substantially less than bulk sound speed. Although Wackerle did not comment on this observation, it is now evident that both sapphire and quartz show similarities in their compressional behaviors in the immediate vicinity of the HEL. Recent piezoelectric response measurements confirm the slow second wave behavior for quartz[38].

(e) *Determination of shear offset*

Although it is not common to do so, the high pressure shock data can be used to give an explicit measure of the shear offset. Under the assumption that all high pressure data points have a constant offset from the isotropic compression curve and that no phase changes have occurred, the high pressure data can be extrapolated to zero stress and the observed offset in relative volume between the extrapolation and the initial relative volume can be used to compute the shear stress offset. By so doing the high pressure shock data may be used as an independent measure of the offset of an anisotropic curve without prejudice as to the nature of the high pressure response. This then provides for an independent comparison of shock data and static data. A schematic of the method for doing this is shown in Fig. 5.

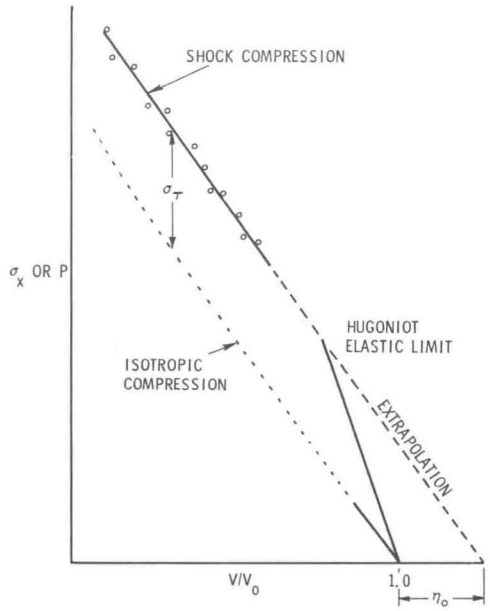

Fig. 5. Extrapolation of high pressure shock data to zero stress may be used to obtain an independent measure of the offset between shock data and the isotropic compression curve. The volume offset at zero stress is a direct measure of the volume offset and the stress offset may be computed as described in the text. The solid depicted responds as an elastic–plastic solid such that $\sigma_\tau = \sigma^*$. The extrapolation does not involve any *a priori* assumptions concerning shear strength and thus may be used as an independent measure of stress offsets.

Assuming that the shear stress offset, σ_τ, is constant for all data above the HEL it can be shown that

$$\sigma_\tau = B\eta_0 \tag{12}$$

where B is the bulk modulus, η_0 is the magnitude of the zero-stress relative volume offset measured from the extrapolation of the high pressure shock data. The bulk modulus must be known but may be determined from data at atmospheric pressure. The change in bulk modulus with pressure will not seriously affect the calculation since only the change in modulus for compressions up to a value equal to the volume offset will affect the calculation.

The zero stress relative volume offset for sapphire is determined from the shock data above the HEL with a cubic polynomial fit to the data. A cubic polynomial expansion about the initial volume, V_0, shows that:

$$1-\frac{V}{V_0} = -\eta_0 + A\sigma - B\sigma^2 + C\sigma^3, \tag{13}$$

where $A = 1/B_0$ and B_0 is the atmospheric pressure bulk modulus. If the bulk modulus is assumed to be linear in pressure; [2]$B = (1+B_0')/2B_0^2$ and $C = (1+3B_0'+2(B_0')^2)/6B_0^3$, where B_0' is the first pressure derivative of the bulk modulus. The adequacy of the cubic polynomial to represent incompressible solids like sapphire in this pressure range has been discussed by Anderson [2].

The best fit for the zero stress volume offset was judged by requiring the first linear term of the polynomial to agree with the ultrasonic measurement of compressibility. The volume offset so obtained is the initial point of a high pressure compression curve fit to the shock data with initial slope in agreement with the ultrasonic data. Iterations are performed in which a volume offset is assumed and fit to the data until agreement with the adiabatic compressibility is obtained. This technique was found to give a volume offset to three significant figures with the present data. Since the coefficient of the second term is related to the pressure derivative of the bulk modulus, B_0', this value is also obtained from the polynomial fit. The values derived for the present shock data are: $\eta_0 = 0{\cdot}0118$, $B_0 = 2{\cdot}542 \times 10^3$ kbar, and $B' = 3{\cdot}69$. Because the compressions are relatively small, these values are representative of adiabatic compressions.

Using a bulk modulus value of $2{\cdot}542 \times 10^3$ kbar [36], the shear stress offset of $\sigma_\tau = 30$ kbar is obtained from equation (12); whereas, the calculated shear strength offset, σ^* from equation (7) has values which range from 55 to 110 kbar.*

From another point of view, the relative volume offset can be used to calculate an HEL value consistent with the elastic–plastic theory and this value can be compared to the measured HEL values. Assuming constant values for bulk modulus, B, and the appropriate one-dimensional strain elastic constant, C, up to compressions to the HEL, it can be shown that if the solid responds as an elastic–plastic solid that:

$$\sigma_\eta = B\eta_0(1-B/C)^{-1} \tag{14}$$

where σ_η is the computed HEL consistent with the observed volume offset and the elastic–plastic model.

The calculated HEL from equation (13) is 60 kbar. This value should be compared to the measured HEL values which range from 120 to 210 kbar. The discrepancy between the HEL predicted from the elastic–plastic theory and the measured values indicates that the elastic–plastic model will not describe the compression of sapphire.

(f) *Summary of shear strength observations*

In summary, it is clear that there are three

*All calculations involving elastic constants in this paper use the data of Gieske and Barsch, Ref. [36]. Their paper also contains an excellent summary of other elastic constant data on Al_2O_3. For the single crystal τ^* was calculated from: $\tau^* = \frac{1}{2}(1-C_{xz}/C_{xx})\sigma_H$, where x is the shock propagation direction and z is the lateral direction and the C's are the elastic stiffness constants.

different interpretations of the shock data which show a substantial loss of shear strength when sapphire is shocked above the HEL. These are:

1. a common high pressure compression curve, independent of the HEL values,
2. shock-velocity values substantially less than local bulk sound speed,
3. and measurements of the volume offset obtained when the high pressure data are extrapolated to zero pressure.

These same criteria are generally applicable to other materials in investigating shear strength effects.

(g) *Comparison with static data*

To this point the conclusions concerning the shear stress offset are based entirely upon the shock data. There are two static pressure measurements which can be used for an independent determination of the high pressure isotropic compression curve. Both of these are shown in Fig. 6.

The compression measurements of Hart and Drickamer[39] were accomplished with X-ray techniques in a high pressure anvil apparatus. Although the measurements show a large experimental error they can be used as a nominal guide to compressions at high pressure.

The most accurate measurements are the ultrasonic wave velocity measurements of Gieske and Barsch[36] to 10 kbar. Although these data must be extrapolated to significantly higher compressions, the determination of higher-order elastic constants in the elastic range show that the bulk modulus and its pressure derivative should give an accurate description of the compression to values used in the present experiments. The comparison of ultrasonic extrapolation and X-ray data show an appreciable difference but the difference is probably within the experimental error of the X-ray measurement.

The temperature rise due to shock compression of sapphire is not appreciable because of

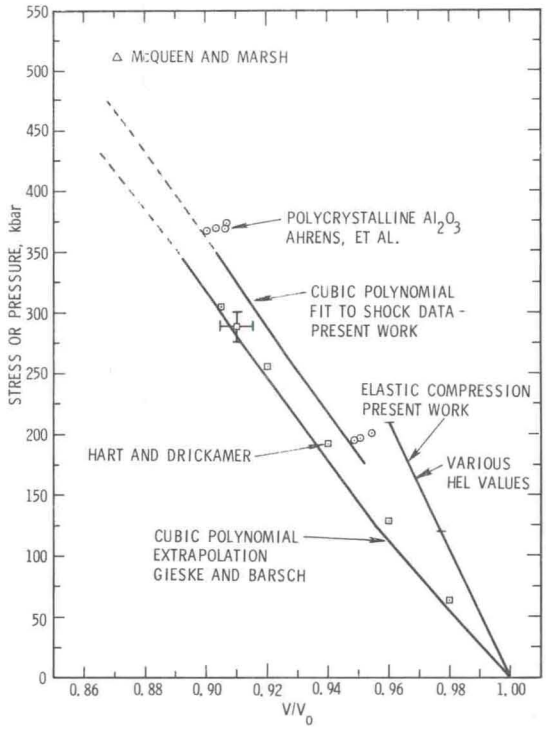

Fig. 6. Compression data for Al_2O_3 derived from various sources. The data obtained in the present investigation is shown by the various polynomial statistical fits. The data of Hart and Drickamer were obtained from lattice parameter determinations. Estimates of their experimental error are shown on one experimental point. The ultrasonic data of Gieske and Barsch measured to 10 kbar are extrapolated with a cubic polynomial to compare to the shock data. The point of McQueen and Marsh for single crystal Al_2O_3 is reported in Ref. [2]. The shock data on a high density Al_2O_3 is shown for comparison with the single crystal data. The cubic polynomial fails to give an accurate representation above a stress of 350 kbar and is shown by a dotted line for comparative purposes only. A logarithmic equation such as a Murnaghan equation gives an excellent correspondence between the data of the present work and that of McQueen and Marsh.

the relatively small compressions involved. Accordingly, the thermal pressure correction computed from conservation of energy is not significant; amounting to about a 6 kbar correction at 400 kbar and about a 1 kbar correction at 150 kbar. These thermal pressure corrections are less than the experimental scatter and small compared to the offset between the static and shock data; hence, the

correction has not been applied to the shock data.

The stress offset observed between the extrapolated ultrasonic data and the best fit to the shock data range from 38 to 43 kbar depending upon the pressure range where the comparisons are accomplished. Likewise the volume offsets are observed to range from 1·1 to 1·3 per cent. Similar offsets to the data of Hart *et al.* are 0·75 to 1·0 per cent and 25 to 38 kbar. These values for stress and volume offsets are in excellent agreement with the values derived from the shock data alone, yet grossly different from values predicted from the elastic–plastic theory and the measured HEL values. Thus, the direct comparison of the static and shock data also demonstrates that when sapphire is shocked to pressures greater than the HEL that a substantial loss of shear strength is observed.

A striking feature of both sapphire and quartz is that both materials show about a 1 per cent volume offset to the isotropic compression curve after a substantial loss of shear strength is experienced. Thus there may be some similarities to the condition of these materials after the loss of shear strength.

Because of the unusual character of the loss of shear strength it is not implausible that the thermodynamic treatment of the yield is inadequate. Unlike yield under elastic–plastic conditions which is analogous to a second order phase transition, the loss of shear strength is analogous to a first-order phase transition. For example, the shear strain elastic energy for sapphire at 200 kbar is 12 cal/g. The loss of shear strength on the time scale of the shock experiments will cause this energy to appear as thermal pressure with an average value of about 6 kbar. Although this pressure is about a factor of five too small to account for the observed difference between static and shock results, the possibility of severe local inhomogeneities due to failure along specific crystallographic planes might cause sufficient complications to cause concern as to the proper treatment of these thermal effects. In any event it appears that more detailed study of possible thermodynamic effects is warranted.

(h) *Hugoniot elastic limit values*

The unusually large HEL values observed for sapphire and the equally unusual loss of shear strength in the high pressure region suggest fundamentally different shear-failure mechanisms than observed for metals. It is, therefore, instructive to compare the maximum shear stress supported by sapphire to predictions of the theoretical shear strength, i.e., the inherent shear strength of the perfect crystal. Present capability for calculating the theoretical shear strength are not sufficiently realistic to give accurate estimates [40, 41]. However, most calculations give a lower bound to the shear strength of about 0·03 G, where G is the appropriate shear modulus. Experimental measurements of values for theoretical shear strength are limited to Brenner's measurements [42] on metallic whiskers which gave values of 0·027 G for Cu, 0·036 G for Au and 0·052 for Fe.

The largest HEL value observed in sapphire was 210 kbar which corresponds to a maximum shear stress of 83 kbar based on the atmospheric pressure elastic constants. This maximum shear stress value is 0·056 C_{44}; large enough to approach estimates of the theoretical shear strengths. The case for quartz is even more noteworthy since the highest HEL observed is 0·11 C_{44}. Thus, both sapphire and quartz exhibit shear strengths under shock compression which could reasonably be theoretical shear strengths and both sapphire and quartz lose shear strength and collapse toward an isotropic compression curve when shocked above the HEL.

On the basis of the limited data it is premature to suggest a general model for the loss of shear strength; however, it is worthwhile to examine the existing shock-compression literature for evidence of large HEL values and shear stress offsets. These data are collected in Table 4. There are reasonably complete

Table 4. Shear strengths of shock loaded crystals

Crystal	Structure	τ_{max}[a] kbar	C_{44} kbar	τ_{max}/C_{44}	Loss of shear strength
SiO_2	Trigonal		579		
Z-cut[24][b]		62		0·108	Yes
X-cut[38]		33		0·057	Yes
Al_2O_3	Trigonal		1472		
0° orientation		83		0·056	Yes
90° orientation		72		0·049	Yes
60° orientation		68		0·046	Yes
MgO[46]	Cubic		1559		Yes? limited
[100]		25		0·016	shock data
TiO_2[47]	Cubic		1239		
[001]		33		0·027	?
[100]		12		0·0096	?
Si[44]	Cubic		796		
[100]		28		0·035	?Yes, possible transition
[111]		12		0·015	No
Ge[111][43]	Cubic	10	672	0·015	No
NaCl[45]	Cubic		128		
[111]		2·3		0·018	Yes? one experiment
[110]		0·28		0·0022	No
[100]		0·09		0·0007	No

[a] τ_{max} is taken to be the maximum observed value of $\frac{1}{2}(\sigma_x - \sigma_y)$, where σ_x is the maximum observed HEL value and σ_y is the minimum lateral stress computed from atmospheric pressure elastic constants. The rationale for taking maximum values is based on the likelihood that the lower values are caused by samples of inferior quality due to internal strains or other defects. In anisotropic crystals lateral stresses may vary due to lateral anisotropy. Because of non steady effects these maximum values may relax to lower stress values.

[b] Reference numbers following the various materials indicate the source for the HEL values used to compute τ_{max}.

data for SiO_2, Al_2O_3, Ge[43], and Si[44] with limited information available for NaCl[45], MgO[27, 46] and TiO_2[27, 47]. One immediate conclusion that can be drawn from an examination of the existing data is that not all solids which are brittle at room temperature and atmospheric pressure exhibit loss of shear strength under shock loading. Furthermore, as previously stated, polycrystalline Al_2O_3, a brittle solid, responds as an elastic–plastic solid. On the other hand, crystalline Al_2O_3 and SiO_2 exhibit a substantial loss of shear strength.

Thus the experimental evidence indicates that a general model proposing that brittle materials lose their shear strength when shocked above the HEL is not suitable to predict material response. Definitions of brittle materials as ordinarily posed are based on crack propagation at stresses less than that necessary to cause slip and inelastic deformation. The large isotropic pressure component of shock experiments will not permit crack propagation; hence, in contrast to static experiments, materials cannot fail by crack propagation and inherent strength properties may be observed in bulk materials.

It appears possible that different shear-failure mechanisms may be encountered in a given crystal shock loaded along different crystallographic axes. If loading is accomplished in a direction which causes no shear on the slip plane, failure cannot be expected by conventional slip mechanisms. Experimental evidence for this is shown in Table 4 where large HEL values are observed in [100] Si and [111] NaCl, while much lower values are observed in other directions. There is

some evidence, admittedly inconclusive, for loss of shear strength in both cases. The [111] NaCl investigation shows one experiment with a wave velocity lower than bulk sound speed. The high pressure [100] Si data show velocities less than bulk sound speed; however, this observation is inconclusive because of the possibility of a phase transition. In any event, the possibility of preferential loss of shear strength in various crystallographic directions in a given crystal should not be overlooked. In fact, it would be highly desirable if various crystals were studied in detail for experimental evidence to examine this question.

The shock compression data[28] on high density polycrystalline Al_2O_3 indicate elastic–plastic response and no loss of shear strength. Although at first glance this seems inconsistent with the results of the present investigation, there is no reason that the yield mechanisms of the polycrystal and single crystal should be the same. In fact, the HEL values for various polycrystalline Al_2O_3 samples as shown in Table 5, show a marked dependence on porosity of the sample. This indicates that the

Table 5. Hugoniot elastic limits of polycrystalline Al_2O_3

Density g cm^{-3}	HEL kbar	Reference
3·98	112 ± 13	28
3·969	70 − 136	29
3·92	140	49
3·81	83 ± 5	28
3·76	58 − 72	20
3·72	80	49

HEL is governed by grain boundary and intergrannular effects and that the shear strength of intergrannular material is apparently less than that required to exceed the shear strength of the crystallite.

The elastic–plastic response of polycrystalline Al_2O_3 and the elastic–isotropic response of single crystal Al_2O_3 support the view that a critical shear stress must be exceeded before a loss of shear strength occurs. Furthermore, this observation indicates that shear strength effects at high pressure are different for polycrystalline and single solids of the same chemical composition.

It seems clear that if slip cannot occur under shock-loading due to an insufficient number of mobile dislocations or due to shear stress of insufficient magnitude on the slip plane, that failure must occur by different mechanisms than ordinarily encountered. The shock data indicate that as the shear stress values approach the theoretical shear stress estimates, substantial loss of shear strength is observed in the high pressure phase. If solids are observed to sustain shear strengths under shock loading which approach or are greater than 0·03 G, a loss of shear strength should be anticipated.

It is perhaps noteworthy that all of the oxides investigated support maximum stress values in excess of 25 kbar and that both of the materials which are known to lose their shear strength are oxides. Since the oxides are known to have elastic properties dependent principally upon the oxygen ion framework [36, 48] the critical shear stress observed for oxides may be a property of the oxygen framework and single crystal oxides are good candidates for materials with large HEL's and a corresponding loss of shear strength.

6. SUMMARY AND CONCLUSIONS

The shock compression data for sapphire show that the compressional behavior of sapphire is analogous to quartz in that both solids exhibit large HEL values and both exhibit a substantial loss of shear strength when shocked above the HEL. Sapphire and quartz are best characterized as elastic–isotropic solids and not elastic–plastic solids. These conclusions are based upon observations of: (1) common high pressure compression curves for various HEL values, (2) high pressure shock velocities less than local bulk sound speed, and (3) the volume

offset when the high pressure data are extrapolated to zero pressure.

Comparison of hydrostatic and shock compression curves for both sapphire and quartz show differences in volume at a given pressure of about 1 per cent. The reason for this is not understood.

The present theoretical and experimental descriptions of yield mechanisms in solids and shear strength effects at high pressure are inadequate to characterize solids other than metals. Brittle material classifications under static conditions do not adequately characterize those materials which are known to respond as elastic–plastic or elastic–isotropic. There is evidence for different shear-failure mechanisms and different shear strength effects between single crystals and polycrystals and for crystals shocked in various crystallographic directions.

When the shear strengths of solids approach the theoretical shear strength values under shock loading, elastic–isotropic response and changes in shear sensitive properties should be anticipated. It is central to our understanding of the compressional behavior of solids under large anisotropic compressions to accomplish further detailed investigations of HEL values and compression curves for stresses immediately above the Hugoniot elastic limit.

Acknowledgement—The authors are pleased to acknowledge many useful discussions with their Sandia Laboratories colleagues, the assistance in the experiments by C. W. Huddle and G. E. Ingram, discussions on elastic–plastic response with R. W. Rohde and J. N. Johnson and methods for statistical fits to the data with A. R. Champion.

REFERENCES

1. DRICKAMER H. G., LYNCH R. W., CLENDENEN R. L. and PEREZ-ALBUERNE E. A., In *Solid State Physics* (Edited by F. Seitz and D. Turnbull), Vol. 19, Academic Press, New York (1966).
2. ANDERSON O. L., *J. Phys. Chem. Solids* **27**, 547 (1966).
3. MCQUEEN R. G. and MARSH S. P., *J. appl. Phys.* **31**, 1253 (1960).
4. RICE M. H., MCQUEEN R. G. and WALSH J. M., In *Solid State Physics* (Edited by F. Seitz and D. Turnbull), Vol. 6, Academic Press, New York (1958).
5. DEAL W. E. JR., In *Modern Very High Pressure Techniques* (Edited by R. H. Wentorf, Jr.), Butterworths, Washington (1962).
6. KARNES C. H., In *Mechanical Behavior of Materials Under Dynamic Loads* (Edited by U. S. Lindholm), Springer-Verlag, New York (1968).
7. GRAHAM R. A., *J. bas. Engng* **89**, 911 (1967).
8. GRAHAM R. A. and HUTCHISON R. E., *Appl. Phys. Lett.* **11**, 69 (1967).
9. WOOD, D. S., *J. appl. Mech.* **19**, 521 (1952).
10. FOWLES G. R., *J. appl. Phys.* **32**, 1475 (1961).
11. LUNDERGAN C. D. and HERRMANN W., *J. appl. Phys.* **34**, 2046 (1963).
12. BARKER L. M., LUNDERGAN C. D. and HERRMANN W., *J. appl. Phys.* **35**, 1203 (1964).
13. BUTCHER B. M. and CANNON J. R., *AIAA Journal* **2**, 2174 (1964).
14. BUTCHER B. M. and MUNSON D. E., In *Proceedings Fourth Symposium on Detonation* ACR-126, Office of Naval Research, U.S. Government Printing Office (1965).
15. BUTCHER B. M. and KARNES C. H., *J. appl. Phys.* **37**, 402 (1966).
16. MUNSON D. E. and BARKER L. M., *J. appl. Phys.* **37**, 1652 (1966).
17. GRAHAM R. A., ANDERSON D. H. and HOLLAND J. R., *J. appl. Phys.* **38**, 223 (1967).
18. HERRMANN W., In *Wave Propagation in Solids*, American Society of Mechanical Engineers, New York (1970).
19. JONES O. E. and GRAHAM R. A., In *Accurate Characterization of the High-Pressure Environment* (Edited by E. C. Lloyd), National Bureau of Standards Special Publication 326, March 1971.
20. See a recent comprehensive summary in GRAHAM R. A. and JONES O. E., Sandia Laboratories Report SC-R-68-1857 (Oct. 1968).
21. JONES O. E., NEILSON F. W. and BENEDICK W. B., *J. appl. Phys.* **33**, 3232 (1962).
22. VAN THIEL M. and KUSUBOV A., In *Accurate Characterization of the High-Pressure Environment* (Edited by E. C. Lloyd), National Bureau of Standards Special Publication 326, March 1971.
23. NEILSON F. W. and BENEDICK W. B., *Bull. Am. phys. Soc.* **5**, 511 (1960); also Sandia Laboratories Report SCR-502 (April 1962).
24. WACKERLE J., *J. appl. Phys.* **33**, 922 (1962).
25. FOWLES G. R., Poulter Laboratories Technical Report 003-61, Stanford Research Institute (1961); also *J. geophys. Res.* **72**, 5729 (1967).
26. DUVALL G. E. and FOWLES G. R., In *High Pressure Physics and Chemistry* (Edited by R. S. Bradley), Vol. 2, Academic Press, New York (1963).
27. AHRENS T. J. and LINDE R. K., In *Behavior of Dense Media Under High Dynamic Pressures*, Gordon and Breach, New York (1968).
28. AHRENS, T. J., GUST W. H. and ROYCE E. B., *J. appl. Phys.* **39**, 4610 (1968).
29. MUNSON D. E., Sandia Laboratories Report SC-RR-69-803 (Jan. 1970).

30. MCWHAN D. B., *J. appl. Phys.* **38**, 347 (1967).
31. BROOKS, W. P. and GRAHAM R. A., *Bull. Am. phys. Soc.* **11**, 414 (1966).
32. GRAHAM R. A. and INGRAM G. E., In *Behavior of Dense Media Under High Dynamic Pressures*, Gordon and Breach, New York (1968).
33. GRAHAM R. A., NEILSON F. W. and BENEDICK W. B., *J. appl. Phys.* **36**, 1775 (1965).
34. INGRAM G. E. and GRAHAM R. A., to be published in *Proceedings Fifth Symposium on Detonation*, Pasadena, Calif. (Aug. 18–21, 1970).
35. HEARMON R. F. S., *An Introduction to Applied Anisotropic Elasticity*, Oxford University Press (1961).
36. GIESKE J. H. and BARSCH G. R., *Phys. Status Solidi* **29**, 121 (1968).
37. BARKER L. M. and HOLLENBACH R. E., *J. appl. Phys.* **41**, 4208 (1970).
38. GRAHAM, R. A. and INGRAM G. E., *Bull. Am. phys. Soc.* **14**, 1163 (1969).
39. HART H. V. and DRICKAMER H. G., *J. chem. Phys.* **43**, 2265 (1965).
40. COTTRELL A. H., *Dislocations and Plastic Flow in Crystals*, Oxford at the Clarendon Press (1958).
41. KELLY A. H., *Strong Solids*, Clarendon Press, Oxford (1966).
42. BRENNER S. S., *J. appl. Phys.* **27**, 1484 (1956), see values given in Ref. [41].
43. GRAHAM R. A., JONES O. E. and HOLLAND J. R., *J. Phys. Chem. Solids* **27**, 151 (1966).
44. GUST W. H. and ROYCE E. B., *J. appl. Phys.* **42**, 1897 (1971).
45. MURRI W. J. and ANDERSON G. D., *J. appl. Phys.* **41**, 3521 (1970).
46. AHRENS T. J., *J. appl. Phys.* **37**, 2532 (1966).
47. LINDE R. K. and DECARLI P. S., *J. chem. Phys.* **50**, 319 (1969).
48. ANDERSON O. L., In *Physical Acoustics* (Edited by W. P. Mason), Vol. III-B, Academic Press, New York (1965).
49. GUST W. H. and ROYCE E. B., *Bull. Am. phys. Soc.* **13**, 901 (1968).

The reviewer called our attention to static compression measurements of C_{111} and C_{333} reported by R. E. Hankey and D. E. Schuele, *J. Acoust. Soc. Am.* **48**, 190 (1970). These authors also report values obtained by J. H. Gieske in a Ph.D. thesis at Penna. State University. The various values are shown below.

Comparison of third-order constants[a]

	Gieske	Hankey *et al.*	Present Work
C_{111}	−3·92	−3·87	−3·6
C_{333}	−3·10	−3·34	−3·6

[a] All units are 10^{13} dyne cm^{-2}.

Differences between the static and shock compression may involve fourth-order constant contributions.